FISEVIER

Contents lists available at ScienceDirect

Acta Materialia

journal homepage: www.elsevier.com/locate/actamat



Full length article

Structural failure of layered thermoelectric $In_4Se_{3-\delta}$ semiconductors is dominated by shear slippage



Min Huang^a, Guodong Li^{a,b,*}, Qi An^c, Pengcheng Zhai^{a,b}, William A. Goddard III^d

- a Hubei Key Laboratory of Theory and Application of Advanced Materials Mechanics, School of Science, Wuhan University of Technology, Wuhan, 430070, PR China
- b State Key Laboratory of Advanced Technology for Materials Synthesis and Processing, Wuhan University of Technology, Wuhan 430070, PR China
- ^c Department of Chemical and Materials Engineering, University of Nevada Reno, Reno, NV 89557, USA
- ^d Materials and Process Simulation Center, California Institute of Technology, Pasadena, CA 91125, USA

ARTICLE INFO

Article History: Received 30 November 2019 Revised 22 January 2020 Accepted 22 January 2020 Available online 27 January 2020

Keywords:
Mechanical properties
Layered In₄Se₃
Fracture mechanism
Strain rate sensitivity
Temperature effect

ABSTRACT

 $In_4Se_{3-\delta}$ semiconductors exhibit high zT as an n-type TE material, making them promising materials for thermoelectric (TE) applications. However, their commercial applications have been limited by the degradation of their mechanical properties upon cyclic thermal loading, making it important to understand their stress response under external loadings. Thus we applied molecular dynamics (MD) simulations using a density functional theory (DFT) derived force field to investigate the stress response and failure mechanism of $In_4Se_{3-\delta}$ under shear loading as a function of strain rates and temperatures. We considered the most plausible slip system (001)/<100> based on the calculations. We find that shear slippage among In/Se layered structures dominates the shear failure of $In_4Se_{3-\delta}$. Particularly, Se vacancies promote disorder of the In atoms in the shear band, which accelerates the shear failure. With increasing temperature, the critical failure strength of In_4Se_3 and the fracture strain of In_4Se_3 decrease gradually. In contrast, the fracture strain of $In_4Se_{3-\delta}$ is improved although the ultimate strength decreases as temperature increases, suggesting that the Se vacancies enhance the ductility at high temperature. In addition, the ultimate strength and the fracture strain for $In_4Se_{2.75}$ increase slightly with the strain rate. This strain rate effect is more significant at low temperature for $In_4Se_{2.75}$ because of the Se vacancies. These findings provide new perspectives of intrinsic failure of $In_4Se_{3-\delta}$ and theory basis for developing robust $In_4Se_{3-\delta}$ TE devices.

© 2020 Acta Materialia Inc. Published by Elsevier Ltd. All rights reserved.

1. Introduction

Thermoelectric (TE) devices can directly convert the heat from automotive exhausts into electricity, which is of great significance for energy sustainability [1,2]. Many efforts have been made to improve the low efficiency of TE energy conversion, which is characterized by the figure of merit, $zT = S^2\sigma T/\kappa$, where S is the Seebeck coefficient, σ is the electrical conductivity, T is the absolute temperature, and κ is the thermal conductivity [2]. The zT could be improved by optimizing the power factor (PF = $S^2\sigma$) and reducing the thermal conductivity (κ) through introducing point and planar defects (vacancies, doping, elemental substitutions and nano-engineering) in various high-performance TE materials such as Mg₂(Si, Ge, Sn) [3–6], CoSb₃ [7–9], Bi₂Te₃ [10–12], PbTe [13–15], SnSe [16–18], Zintl phases [19,20], and Half-Heusler alloys [21–23]. The engineering application of TE materials requires mechanical robustness that can undergo cycling thermal stress in a temperature gradient and can resist crack opening

 $\label{lem:email$

or failure of devices from vibrations. Unfortunately, thermo-mechanical loadings can cause the degeneration of the mechanical properties, leading to the failure of TE devices [24–27]. Thus, it is essential to obtain an in-depth understanding of how mechanical properties of these TE materials behave in engineering applications.

A TE device requires one p-type and one n-type leg which are equally important for engineering applications. The n-type TE material $In_4Se_{3-\delta}$ (self-doping by Se deficiency) was reported as a promising candidate for applications in the mid-temperature range (500 to 900 K) with a zT value of 1.48 at 705 K. This high zT value is attributed to its highly anisotropic crystal structure arising from a disordered two-dimensional crystalline sheets coupled with a charge density wave (CDW) instability arising from its distinctive electronic structure [28–30]. Many efforts have been made to improve the thermoelectric and mechanical properties of In₄Se_{3-δ}. Zhu et al. [31] reported that the electrical conductivity and thermal conductivity of polycrystalline In₄Se_{3-δ} compounds can be controlled by adjusting Se vacancies, with the zT value reaching ~1.0 for δ = 0.65 and 0.8. Li et al. successfully strengthened the flexural strength of In₄Se_{2.65} TE material by 40% through introducing the uniformly distributed TiC nanoparticles into In₄Se_{2.65} composites [32]. In addition, many theoretical

^{*} Corresponding authors.

predictions have been made on the electronic and thermal transport properties of $\ln_4 Se_{3-\delta}$. Thus, Luo et al. [33] used first-principles simulations to show that the site and concentration of Se vacancies strongly effects the thermoelectric performance of $\ln_4 Se_3$. Ji et al. [28] used molecular dynamics (MD) simulations to find that phonon propagation is strongly dependent on the Se deficiency along the $\ln Se$ chain direction, which is pivotal in optimizing TE performance.

We have applied density functional theory to determine that the $(001)/{<}100{>}$ is the easiest slip system of In_4Se_3 under shear stress among these slip systems $((001)/{<}100{>}, (100)/{<}010{>}, (010)/{<}001{>}, (110)/{<}100{>}$ and $(-110)/{<}110{>})$ [34]. Nevertheless, such DFT studies are limited to hundreds of atoms and zero temperature so that the intrinsic failure mechanism of In_4Se_3 at higher temperatures as a function of Se deficiency and strain rate remains unknown.

This work determines the deformation mechanism of the $In_4Se_{3-\delta}$ TE materials under shear loading along (001)/<100> slip system, including the effects of temperature and strain rate. Applying large-scale MD simulations to finite shear deformation on single crystal $In_4Se_{3-\delta}$ along the (001)/<100> slip system, we find shear slippage in In/Se layered structures dominates the shear fracture of $In_4Se_{3-\delta}$ and that Se vacancies accelerate this failure process. Increasing temperatures have a dramatic influence on the ultimate strength and the fracture strain. The strain rate has a slight effect on the mechanical properties but it is more significant at low temperature for $In_4Se_{2.75}$ because of the presence of Se vacancies.

2. Methodology

All MD simulations were conducted using the large-scale atomic/ molecular massive parallel simulator (LAMMPS) open-source software [35,36]. The atomic interaction in In₄Se₃ were described using the force field developed previously. A Morse bond term was used to describe the valence pair interactions and the cosine-squared angle term was applied to describe the three-body interactions. The elastic properties and thermal conductivity of In₄Se₃ are predicted accurately using this force field [28]. The isothermal-isobaric (NPT) ensemble was applied to relax the structures at various temperature before shear deformation. The temperatures and pressures were adjusted using the Nose-Hoover thermostat and barostat, with the damping parameters of 300–900 K (300 K, 500 K, 700 K, and 900 K) and 0 GPa for temperature and pressure, respectively. Periodic boundary conditions (PBC) were applied to all three directions with a timestep of 0.001 picosecond. The initial atomic velocities were created using the Maxwell-Boltzmann distribution at various temperatures (300 K, 500 K, 700 K and 900 K). These systems were relaxed for 100 ps at each temperature to reach an equilibrium state. The atomic configuration is depicted using the Open Visualization Tool (OVITO) [37–39].

We performed shear deformation simulations on a 10 \times 10 \times 40 supercell (101,200–112,000 atoms) with cell parameters of a = 153.38 Å, b = 123.41 Å and c = 163.68 Å. We considered the (001)/<100> slip system with the shear loading performed by changing the angle between the a and c axes. The canonical (NVT) ensemble was used in the shear deformation. The applied shear strain is the engineering strain and the shear stress is computed from the summation of atomic stress (virial stress) over the system. The temperature was kept at 300 K, 500 K, 700 K and 900 K, respectively, to examine the temperature effect and the strain rates were set at 10^7 s $^{-1}$, 5×10^7 s $^{-1}$, 1×10^8 s $^{-1}$, 5×10^8 s $^{-1}$ and 1×10^9 s $^{-1}$ respectively to examine the effect of strain rate.

3. Results and discussion

3.1. Atomic structure of In₄Se_{3-δ}

The In_4Se_3 binary compound crystallizes in the *Pnnm* orthorhombic space group (No. 58) with 28 atoms per cell (see Fig. 1a). It has lattice parameters of a=15.297 Å, b=12.308 Å, and c=4.081 Å [40,41]. The In1, In2 and In3 atoms as $In^{1.667+}$ form In-In metallic bonds (2.77 Å

average) which connect to Se atoms by In-Se covalent bonds (2.62 to 2.80 Å). This forms the In/Se layered structures stacked along the $\langle 100 \rangle$ direction by van der Waals forces. Specifically, the structure is composed of concatenate In/Se chains running along the (001) direction. These In/Se chains are distorted to form five-membered In/Se pentagon frameworks in the ab plane that are connected by In1-In2 bonds (2.78 Å) to form In/Se layered structures along the (100) direction. The In 4 atom, an In tation, strengthens the van der Waals layer-layer interaction by a weak ionic bond, with the bond lengths of 3.39 Å, 3.16 Å and 2.97 Å for In4-Se1, In4-Se2 and In4-Se3 respectively. Detailed atomistic structures are given in Fig. 1a to illustrate the atomic trajectory and depicts atomic positions of the In/Se chains, the In/Se pentagon frameworks, the In1-In2-In3 trios and the In4 atoms in ab and ac planes. Furthermore, we find that the Se3 atom is the most probable vacancy sites for the lowest formation energy [28,30]. Thus, we created vacancies at Se3 site randomly in our systems. The radial distribution function (RDF) (see Fig. 1b) shows that the structures of $In_4Se_{3-\delta}$ remain stable at room temperature (300 K), which is above Debye temperature of ~73.7 K.

3.2. Fracture mechanism of single crystalline $In_4Se_{3-\delta}$

Fig. 2 shows the stress-strain curves of $\ln_4 Se_{3-\delta}$ at room temperature (300 K) with a strain rate of 10^8 s $^{-1}$ (δ = 0, 0.05, 0.15, 0.25, 0.35, 0.5, 0.625, 0.675) under shear loading along the (001)/<100> slip system. With the increase of Se vacancies, the ultimate strength of $\ln_4 Se_{3-\delta}$ decreases from 7.10 to 3.17 GPa, suggesting that the Se vacancy weakens the structure and decreases the strength. Moreover the fracture strain also decreases from 0.2098 to 0.1364, indicating that Se vacancy has a negative effect on the ductility. We note that the slope of the stress-strain curves (elastic modulus) drops by 9.59–39.34% as the value of δ increases from 0.05 to 0.675. These results indicate that the ultimate strength of TE material $\ln_4 Se_{3-\delta}$ is sensitive to vacancies. Thus, increased vacancy concentrations lead to detrimental changes in mechanical properties.

To determine the failure mechanism of $In_4Se_{3-\delta}$, we focused on the shear deformation process of In₄Se₃ and In₄Se_{2,325} and visualized the atomistic configurations at critical strains, as shown in Fig. 3 and Fig. S1 (in Supplementary material). Detailed atomistic structures are given to illustrate the atomic trajectory and to show atomic positions of the In/Se chains, the In/Se pentagon frameworks, the In1-In2-In3 trios and the In4 atoms. For the perfect bulk In₄Se₃, shown in Fig. 3a and b, the whole structure retains its integrity as the shear strain increases to 0.2094. When the shear strain further increases to 0.2096, (Fig. 3c and d), the cracks occur between In/Se layered structures. Because of the weak van der Waals intra-layer interaction, slippage of In/Se layered structures is most likely to be activated to resist deformation. Meanwhile, the In/Se chains, the In/Se pentagon frameworks, and the In1-In2-In3 trios remain intact, which is attributed to the much stronger interaction between In/Se sub-structures compared with the van der Waals intra-layer interaction. Furthermore, as shown in Fig. 3d, ionic In4-Se bonds were stretched and broken to release shear stress. As the shear strain increases to 0.2098 (Fig. 3e and f), In/Se layered structures further slip along the c-axis, leading to the shear band formation. This gives rise to a high potential energy of the In4 and Se atoms near the shear band region (Fig. S2a). In₄Se_{2,325} with Se3 deficiency shows a deformation mechanisms similar to ideal In₄Se₃, as shown in Fig. S1 (a-f). However, the Se3 deficiency leads to the structural rigidity of In₄Se_{2,325} much weaker than that of the ideal bulk, accelerating slippage and shear band formation. When the shear strain reaches 0.1360, In/Se layered structures start to slip and some In4 atoms disorder with slight distortion of In/Se chains and In/Se pentagon frameworks. A shear band with high atomic potential energies for the In4 and Se atoms forms at 0.1364 shear strain (Fig. S2b). These critical shear strain values are much smaller than those (0.2094 and 0.2098 shear strains) in perfect In₄Se₃.

We explored the structural changes through computing the RDF of ln_4Se_3 at shear strains of 0, 0.2096 and 0.2099 as well as $ln_4Se_{2.325}$

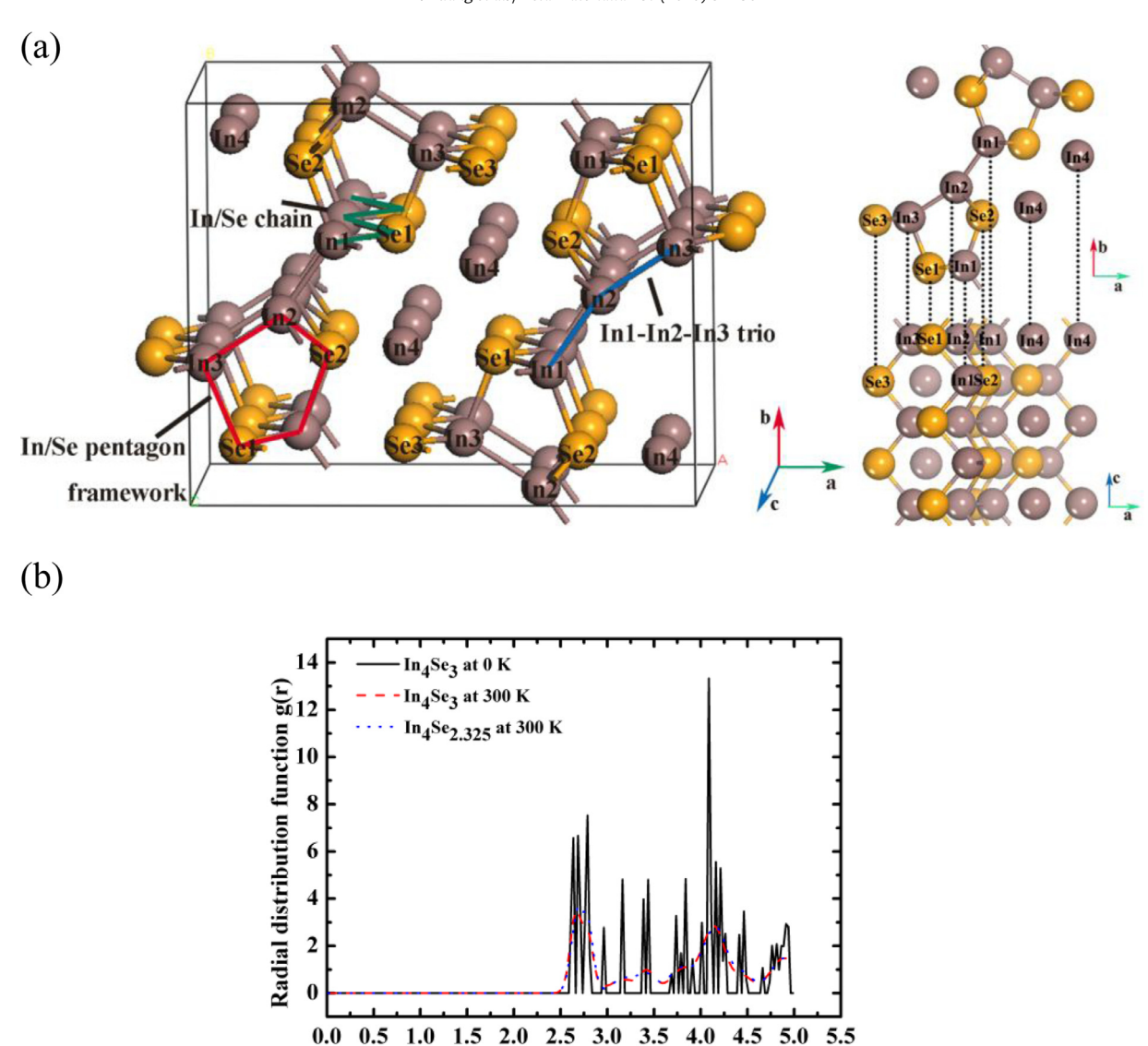


Fig. 1. (a) Atomic structure of In₄Se₃ and a, b, c represent (100), (010) and (001) crystallographic orientations respectively; (b) RDF of In₄Se₃ and In₄Se_{2,325} at 0 K and 300 K, respectively.

Radius (Å)

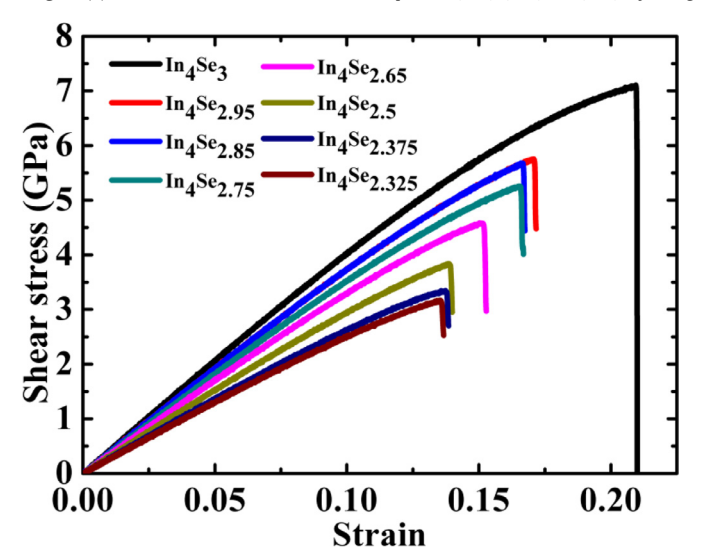


Fig. 2. Stress-strain curves of single crystalline $In_4Se_{3-\delta}$ with a strain rate of 10^8 s $^{-1}$ under shear loading along the (001)/<100> slip system at 300 K. Thus increased vacancies reduce the strength. (For interpretation of the references to colour in this figure legend, the reader is referred to the web version of this article.)

at shear strains of 0.1360 and 0.1368 at room temperature, as shown in Fig. 4 and Fig. S3, respectively. All RDF spectrums show a strong peak located at ~2.68 Å, corresponding to lengths of In-Se covalent bonds and In-In metallic bonds which consist of the In/Se chains, the In/Se pentagon frameworks and the In1-In2-In3 trios. This unchanged peak indicates that the In/Se sub-structure (the In/Se chains, the In/Se pentagon frameworks and the In1-In2-In3 trios) keeps intact in the process of shear deformation, which is consistent with the atomic configuration analysis above. For the single crystal In₄Se₃, the peaks of In₄-Se₁, In₄-Se₂ and In₄-Se₃) and In₄-In 4 (0 shear strain) collapse into a weak one at shear strain of 0.2096, as shown in RDF spectrums. This indicates that the weak In4-Se ionic bonds break with the slippage of In/Se layered structures. Some small peaks emerge from 0 to 2.3 Å at the shear strain of 0.2099, suggesting the formation of shear band and structural breakage. This agrees well with the atomic disorder characteristic in the region of shear band (Fig. 3f). In addition, for In₄Se_{2,325} with Se3 vacancies (Fig. S3), the second peak becomes smooth, accounting for the slippage and disorder of In/Se layered structures. This represents the In4-Se breakage and structural distortion at shear strain of 0.1360 (Fig. S3d). It is worth noting that the small peak of Se3-Se3 disappears, which arises from Se3 vacancies in the In₄Se_{2.325} systems, rather than bond

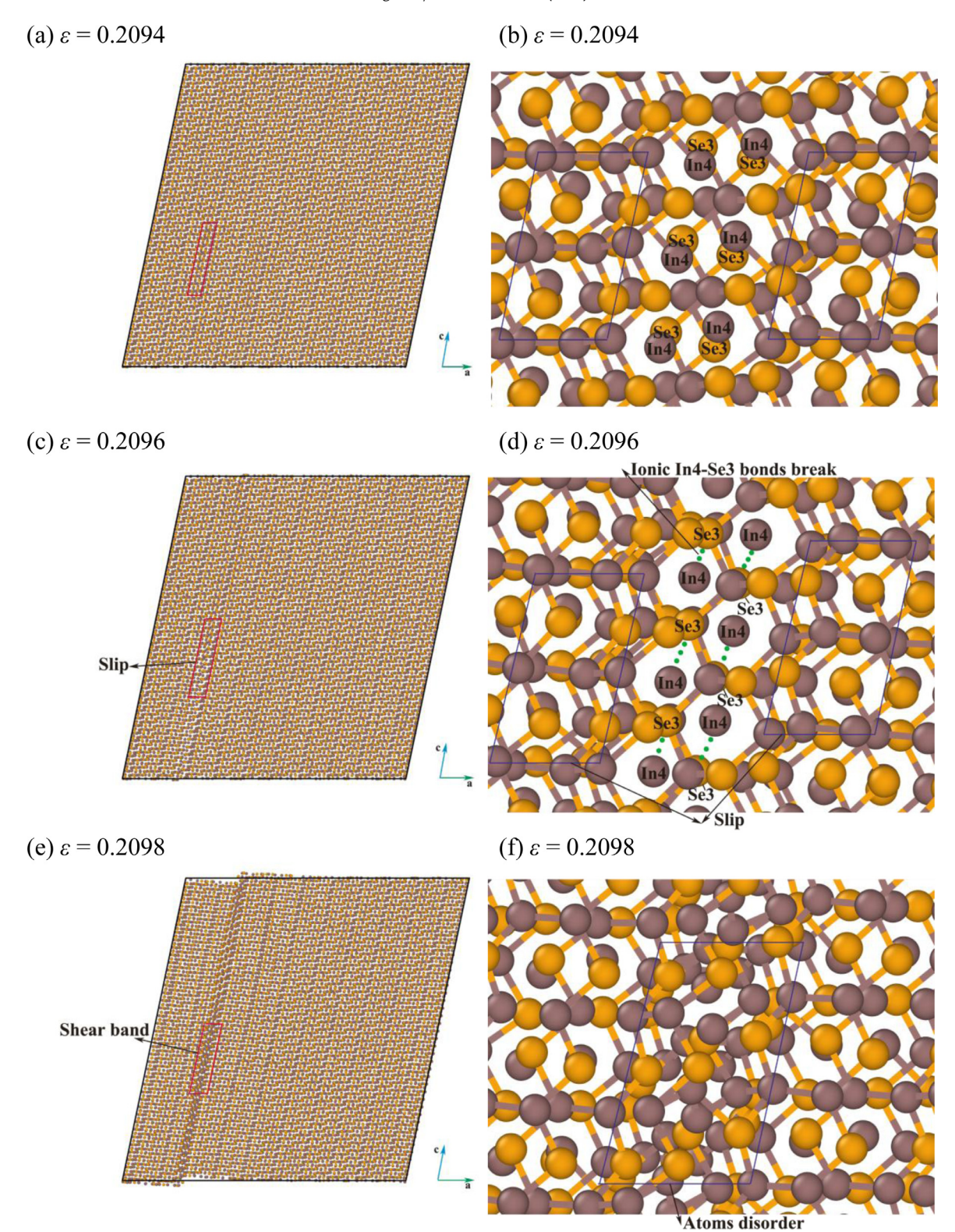


Fig. 3. Snapshots of \ln_4 Se₃ under shear loading along (001)/<100> slip system showing the deformation process about slipping among $\ln/$ Se layered structures without the breakage of the $\ln/$ Se chains, the $\ln/$ Se pentagon frameworks or the $\ln-$ 1n2- \ln 3 trios. (a and b) The atomistic configuration at 0.2094 shear strain. (c, d) The atomistic configuration at 0.2096 shear strain. (For interpretation of the references to colour in this figure legend, the reader is referred to the web version of this article.)

breakage. When the shear strain increases to 0.1364, a shear band forms and the structure of $In_4Se_{2.325}$ fails with weak peaks emerging from 0 to 2.3 Å, which is similar to the RDF in ideal In_4Se_3 .

To further reveal the shear fracture mechanism, we analyzed the average shear stress and density of In_4Se_3 and $In_4Se_{2.325}$ within each bin during the shear process, as shown in Fig. 5 and Fig. S4, respectively. The

whole simulation model is partitioned into 10 bins along $\langle 100 \rangle$ direction for shearing along (001)/<100> slip system (Fig. 5a and Fig. S4a). For In₄Se₃, the shear stress and density keep unchanged at the 0.2094 shear strain, indicating that the whole structure remains its integrity. With increasing shear strain of 0.2096, the In/Se layered structures slip accompanied with slight reduction of shear stress and stabilization of density.

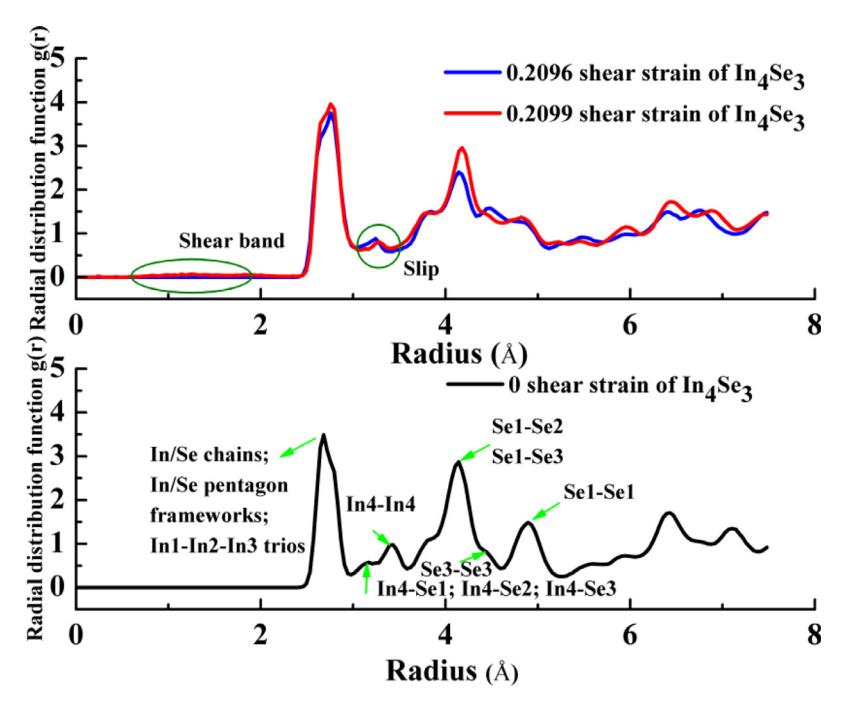


Fig. 4. The RDF of the In_4Se_3 at 0, 0.2096 and 0.2099 shear strains.

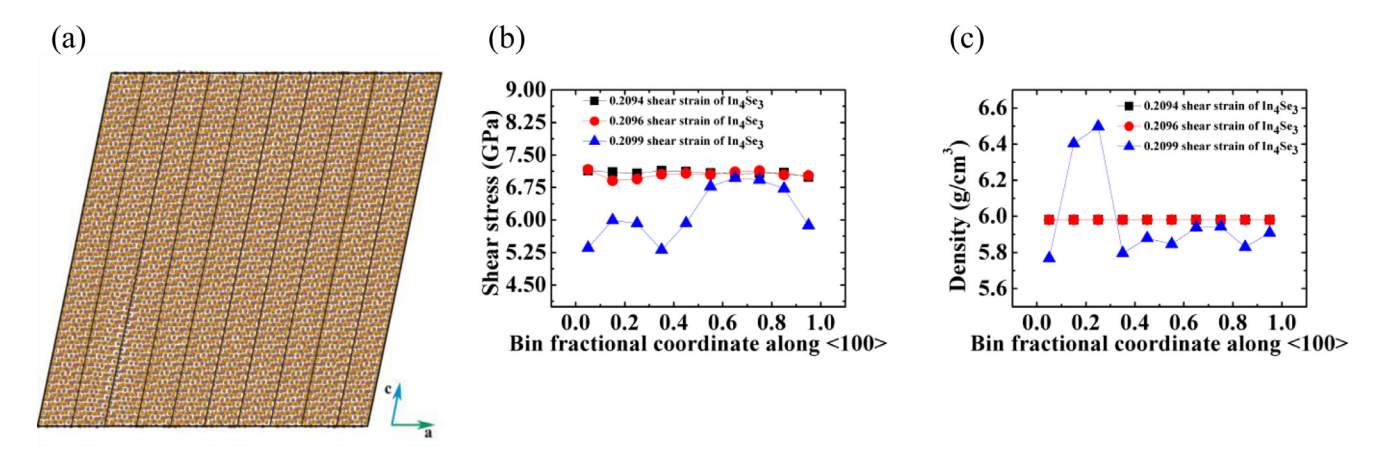


Fig. 5. The shear stress and density analysis for shear fracture mechanism of In_4Se_3 under shear loading along (001)/<100> slip system. (a) The snapshot of In_4Se_3 at shear strain of 0.2096 with the 1-dimensional bin partitioned by black lines along (100). (b) The shear stress profile along (100) at 0.2094, 0.2096, and 0.2099 shear strains. (c) The density profile along (100) at 0.2094, 0.2096, and 0.2099 shear strains.

This indicates that the In/Se sub-structures (the In/Se chains, the In/Se pentagon frameworks and the In1-In2-In3 trios) maintain unchanged with the breakage of weak In4-Se ionic bonds. When the shear strain increases to 0.2099, the shear band forms randomly within 10 bins leading to a released shear stress and a dramatically increased density, representing the atomic disorder. These findings match the results of the atomic configuration analysis and the RDF spectrums. For $In_4Se_{2.325}$ with Se3 vacancies, the fracture mechanism is similar with that in In_4Se_3 system. However, the formation of shear band and atomic disorder starts from the low density atomic region.

3.3. Effect of strain rate and temperature on mechanical properties of single crystalline $In_4Se_{3-\delta}$

Finally, we studied the effects of strain rate $(10^7-10^9~s^{-1})$ and temperature (300 to 900 K) on mechanical properties of single crystalline $In_4Se_{3-\delta}$ under shear loading along (001)/<100> slip system, as shown in Fig. 6a and b. Both ultimate strength and fracture strain slightly increase with increasing strain rate for In_4Se_3 and $In_4Se_{2.75}$, while the elastic modulus is independent of the

strain rate. The ultimate strength and the elastic modulus of $In_4Se_{3-\delta}$ reduces resulting from drastic atom motion at high temperature. With the increased temperature, the fracture strain of $In_4Se_{2.75}$ shows an incremental tendency, while the fracture strain of In_4Se_3 decreases.

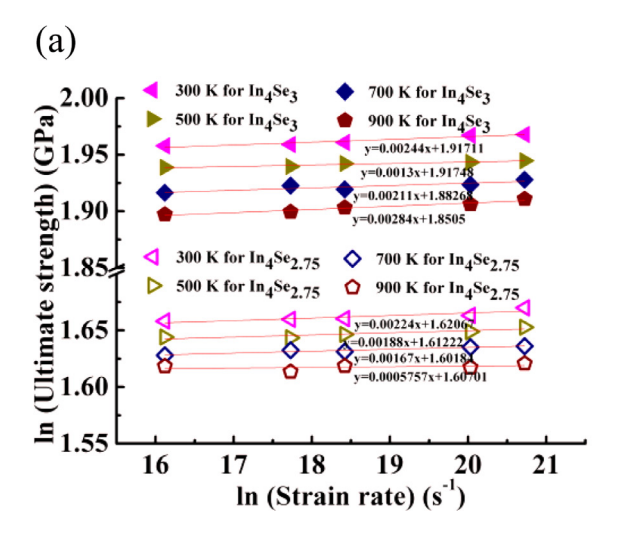
The relationship between fracture strength and strain rate can be depicted by [42,43]:

$$\dot{\varepsilon} = A\sigma^n \exp\left(-\frac{Q}{RT}\right) \tag{1}$$

Where \dot{e} is the strain rate; σ is the fracture strength; Q, R and T relate to intrinsic properties of materials; A is a constant; n is relative to strain-rate sensitivity. Taking natural logarithm from both sides of Eq. (1), we get:

$$\ln \sigma = \ln C + m \ln \dot{\varepsilon} \tag{2}$$

Where m=1/n called the strain rate sensitivity. And C is relative to the Q, R, T and A. Thus, the slope of $\ln{(\dot{\varepsilon})}$ - $\ln{(\sigma)}$ curve represents the strain-rate sensitivity m. This indicates that the plot of $\ln{\sigma}$ as a function of $\ln{\dot{\varepsilon}}$ should be linear.



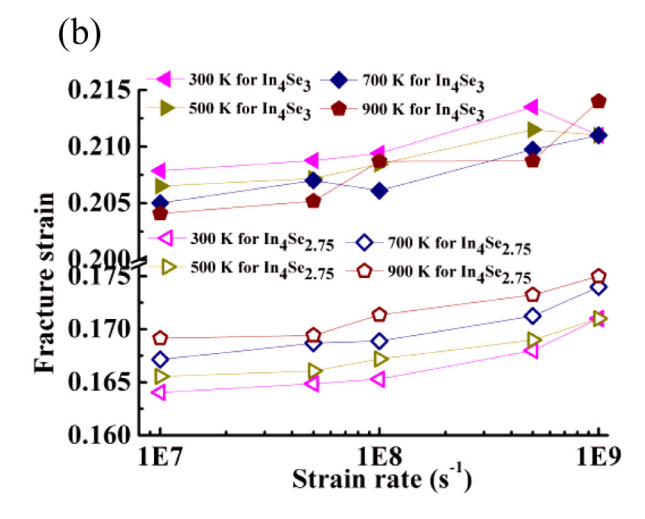


Fig. 6. The relationships between strain rate and mechanical properties of In_4Se_3 and $In_4Se_{2.75}$ at temperature from 300 K to 900 K, including the ultimate strength (a) and the fracture strain (b), respectively.

As shown in Fig. 6a, the strain rate sensitivity of ideal In_4Se_3 is within a narrow range of 1.30×10^{-3} to 2.84×10^{-3} from 300 to 900 K, which means that the strain rate sensitivity is independent of temperature. However, for $In_4Se_{2.75}$ with Se3 vacancies, the strain rate sensitivity increases from 0.58×10^{-3} to 2.24×10^{-3} at temperatures ranging from 300 to 900 K, indicating that the strain rate is more significant in influencing the mechanical properties of $In_4Se_{2.75}$ at lower temperature.

There are many elements that can improve the TE properties of In_4Se_3 , such as Cl, Ag, Pb, Yb, Na, Ca elements [44–46]. Our group is now investigating the effect of element doping on the mechanical properties of In_4Se_3 materials using quantum mechanics. Furthermore, we are constructing the classical interatomic potentials of In_4Se_3 doping with various elements through fitting a potential energy surface on the basis of density function theory. Then, we will conduct some large-scaled molecular dynamics studies on the deformation and failure mechanism of doped In_4Se_3 -based materials.

4. Conclusion

In summary, we employed MD simulations to investigate the fracture mechanism of layered thermoelectric $In_4Se_{3-\delta}$ under shear loading along the most plausible (001)/<100> slip system. We found that the shear slippage among In/Se layered structures dominates the structural destruction in $In_4Se_{3-\delta}$ systems, while the In/Se sub-structures (the In/Se chains, the In/Se pentagon frameworks and the In1-In2-In3 trios) remain intact. The Se vacancies soften the structure and weaken the mechanical properties of single crystalline $In_4Se_{3-\delta}$. This derives from the atomic disorder of the In and Se atoms that can accelerate the shear slippage and structural failure.

In addition, the ultimate strength and the fracture strain increase slightly at high strain rate for In_4Se_3 and $In_4Se_{2.75}$ while the elastic modulus is unaffected. The ultimate strength and the elastic modulus of $In_4Se_{3-\delta}$ reduce at high temperature. However, with the increased temperature, the fracture strain of $In_4Se_{2.75}$ shows an incremental tendency, while the fracture strain of In_4Se_3 decreases. The strain rate sensitivity is more significant at low temperature for $In_4Se_{2.75}$. But it is temperature-independent for ideal bulk In_4Se_3 .

Declaration of Competing Interest

The authors declare that they have no known competing financial interests or personal relationships that could have appeared to influence the work reported in this paper.

Acknowledgements

This work was supported by the National Natural Science Foundation of China (No. 51972253, 51772231); the Hubei Provincial Natural Science Foundation of China (2018CFB646); and the Fundamental Research Funds for the Central Universities (No. WUT 2019IVA055, 2019IB006). We acknowledge Sandia National Laboratories for distributing the open-source MD software LAMMPS. Wag was supported by the US NSF (CBET-1805022).

Supplementary materials

Supplementary material associated with this article can be found in the online version at doi:10.1016/j.actamat.2020.01.045.

References

- [1] P. Ren, Y. Liu, J. He, T. Lv, J. Gao, G. Xu, Recent advances in inorganic material thermoelectrics, Inorg. Chem. Front. 5 (2018) 2380–2398, doi: 10.1039/c8qi00366a.
- [2] J.S. Rhyee, K.H. Lee, S.M. Lee, E. Cho, S.I. Kim, E. Lee, Y.S. Kwon, J.H. Shim, G. Kotliar, Peierls distortion as a route to high thermoelectric performance in In₄Se_{3-δ} crystals, Nature 459 (2009) 965–968, doi: 10.1038/nature08088.
- [3] J.J. Pulikkotil, D.J. Singh, S. Auluck, M. Saravanan, D.K. Misra, A. Dhar, R.C. Budhani, Doping and temperature dependence of thermoelectric properties in Mg₂(Si,Sn), Phys. Rev. B 86 (2012) 155204, doi: 10.1103/PhysRevB.86.155204.
- [4] H.Y. Chen, N. Savvides, Microstructure and thermoelectric properties of n- and ptype doped Mg₂Sn compounds prepared by the modified bridgman method, J. Electron. Mater. 38 (2009) 1056–1060, doi: 10.1007/s11664-008-0630-1.
- [5] X.J. Tan, G.Q. Liu, H.Z. Shao, J.T. Xu, B. Yu, H.C. Jiang, J. Jiang, Acoustic phonon softening and reduced thermal conductivity in Mg₂Si_{1-x}Sn_x solid solutions, Appl. Phys. Lett. 110 (2017) 143903, doi: 10.1063/1.4979871.
- [6] D. Zhou, J. Liu, S. Xu, P. Peng, Thermal stability and elastic properties of Mg₂X (X=Si, Ge, Sn, Pb) phases from first-principle calculations, Comput. Mater. Sci. 51 (2012) 409–414, doi: 10.1016/j.commatsci.2011.07.012.
- [7] Y. Tang, Z.M. Gibbs, L.A. Agapito, G. Li, H.S. Kim, M.B. Nardelli, S. Curtarolo, G.J. Snyder, Convergence of multi-valley bands as the electronic origin of high thermoelectric performance in CoSb₃ skutterudites, Nat. Mater. 14 (2015) 1223–1228, doi: 10.1038/nmat4430.
- [8] R. Guo, X. Wang, B. Huang, Thermal conductivity of skutterudite CoSb₃ from first principles: substitution and nanoengineering effects, Sci. Rep. 5 (2015) 7806, doi: 10.1038/srep07806.
- [9] L. Xi, Y. Qiu, S. Zheng, X. Shi, J. Yang, L. Chen, D.J. Singh, J. Yang, W. Zhang, Complex doping of group 13 elements In and Ga in caged skutterudite CoSb₃, Acta Mater 85 (2015) 112–121. doi: 10.1016/i.actamat.2014.11.022.
- 10] Y. Liu, M. Zhou, J. He, Towards higher thermoelectric performance of Bi₂Te₃ via defect engineering, Scr. Mater. 111 (2016) 39–43, doi: 10.1016/j.scriptamat.2015.06.031.
- [11] Y. Pan, T.-.R. Wei, C.-.F. Wu, J.-.F. Li, Electrical and thermal transport properties of spark plasma sintered n-type Bi₂Te_{3-..}Se_x alloys: the combined effect of point defect and Se content, J. Mater. Chem. C 3 (2015) 10583–10589, doi: 10.1039/c5tc02219c.
- [12] L. Yang, Z.G. Chen, M. Hong, G. Han, J. Zou, Enhanced thermoelectric performance of nanostructured Bi₂Te₃ through significant phonon scattering, ACS Appl. Mater. Interfaces 7 (2015) 23694–23699, doi: 10.1021/acsami.5b07596.

- [13] J. Zhang, D. Wu, D. He, D. Feng, M. Yin, X. Qin, J. He, Extraordinary thermoelectric performance realized in n-Type PbTe through multiphase nanostructure engineering, Adv. Mater. (2017) 29, doi: 10.1002/adma.201703148.
- [14] L. Yang, Z.-G. Chen, M. Hong, L. Wang, D. Kong, L. Huang, G. Han, Y. Zou, M. Dargusch, J. Zou, n-type bi-doped PbTe nanocubes with enhanced thermoelectric performance, Nano Energy 31 (2017) 105–112, doi: 10.1016/j.nanoen.2016.11.027.
- [15] K. Zhang, Q. Zhang, L. Wang, W. Jiang, L. Chen, Enhanced thermoelectric performance of Se-doped PbTe bulk materials via nanostructuring and multi-scale hierarchical architecture, J. Alloys. Compd. 725 (2017) 563–572, doi: 10.1016/j. iallcom.2017.07.193.
- [16] L.-D. Zhao, G. Tan, S. Hao, J. He, Y. Pei, H. Chi, H. Wang, S. Gong, H. Xu, V.P. Dravid, Ultrahigh power factor and thermoelectric performance in hole-doped singlecrystal SnSe, Science 351 (2016) 141–144, doi: 10.1126/science.aad3749.
- [17] A.T. Duong, V.Q. Nguyen, G. Duvjir, V.T. Duong, S. Kwon, J.Y. Song, J.K. Lee, J.E. Lee, S. Park, T. Min, J. Lee, J. Kim, S. Cho, Achieving ZT=2.2 with bi-doped n-type SnSe single crystals, Nat. Commun. 7 (2016) 13713, doi: 10.1038/ncomms13713.
- [18] J.C. Li, D. Li, X.Y. Qin, J. Zhang, Enhanced thermoelectric performance of p-type SnSe doped with Zn, Scr. Mater. 126 (2017) 6–10, doi: 10.1016/j.scriptamat.2016.08.009.
- [19] S.R. Brown, S.M. Kauzlarich, F. Gascoin, G.J. Snyder, YbMnSb: new high efficiency thermoelectric material for power generation, Chem. Mater. 18 (2006) 1873– 1877, doi: 10.1021/cm060261t.
- [20] E.S. Toberer, S.R. Brown, T. Ikeda, S.M. Kauzlarich, G. Jeffrey Snyder, High thermoelectric efficiency in lanthanum doped Yb₁₄MnSb₁₁, Appl. Phys. Lett. 93 (2008) 062110. doi: 10.1063/1.2970089.
- [21] Y. Kimura, T. Tanoguchi, T. Kita, Vacancy site occupation by Co and Ir in half-Heusler ZrNiSn and conversion of the thermoelectric properties from n-type to p-type, Acta Mater. 58 (2010) 4354–4361, doi: 10.1016/j.actamat.2010.04.028.
- [22] C.S. Birkel, W.G. Zeier, J.E. Douglas, B.R. Lettiere, C.E. Mills, G. Seward, A. Birkel, M.L. Snedaker, Y. Zhang, G.J. Snyder, T.M. Pollock, R. Seshadri, G.D. Stucky, Rapid microwave preparation of thermoelectric TiNiSn and TiCoSb half-Heusler compounds, Chem. Mater. 24 (2012) 2558–2565, doi: 10.1021/cm3011343.
- [23] J. Yang, H. Li, T. Wu, W. Zhang, L. Chen, J. Yang, Evaluation of half-Heusler compounds as thermoelectric materials based on the calculated electrical transport properties, Adv. Funct. Mater. 18 (2008) 2880–2888, doi: 10.1002/adfm.200701369.
- [24] D. Zhao, H. Geng, L. Chen, Microstructure contact studies for skutterudite thermoelectric devices, Int. J. Appl. Ceram. Technol. 9 (2012) 733–741, doi: 10.1111/ i.1744-7402.2011.02703.x.
- [25] G. Rogl, A. Grytsiv, M. Gürth, A. Tavassoli, C. Ebner, A. Wünschek, S. Puchegger, V. Soprunyuk, W. Schranz, E. Bauer, H. Müller, M. Zehetbauer, P. Rogl, Mechanical properties of half-Heusler alloys, Acta Mater. 107 (2016) 178–195, doi: 10.1016/j.actamat.2016.01.031.
- [26] G. Li, Q. An, W.A. Goddard, R. Hanus, P. Zhai, Q. Zhang, G.J. Snyder, Atomistic explanation of brittle failure of thermoelectric skutterudite CoSb₃, Acta Mater. 103 (2016) 775–780, doi: 10.1016/j.actamat.2015.11.021.
- [27] G. Li, U. Aydemir, B. Duan, M.T. Agne, H. Wang, M. Wood, Q. Zhang, P. Zhai, W.A. Goddard III, G.J. Snyder, Micro- and macromechanical properties of thermoelectric lead chalcogenides, ACS Appl. Mater. Interfaces 9 (2017) 40488–40496, doi: 10.1021/acsami.7b15651.
- [28] H.S. Ji, H. Kim, C. Lee, J.-.S. Rhyee, M.H. Kim, M. Kaviany, J.H. Shim, Vacancy-suppressed lattice conductivity of high-ZT In₄Se_{3-x}, Phys. Rev. B 87 (2013) 125111, doi: 10.1103/PhysRevB.87.125111.

- [29] L. Makinistian, E.A. Albanesi, N.V. Gonzalez Lemus, A.G. Petukhov, D. Schmidt, E. Schubert, M. Schubert, Y.B. Losovyj, P. Galiy, P. Dowben, Ab initio calculations and ellipsometry measurements of the optical properties of the layered semiconductor In₄Se₃, Phys. Rev. B 81 (2010) 075217, doi: 10.1103/PhysRevB.81.075217.
- [30] X. Yin, J.Y. Liu, L. Chen, L.M. Wu, High thermoelectric performance of In₄Se₃-based materials and the influencing factors, Acc Chem. Res. 51 (2018) 240–247, doi: 10.1021/acs.accounts.7b00480.
- [31] G.H. Zhu, Y.C. Lan, H. Wang, G. Joshi, Q. Hao, G. Chen, Z.F. Ren, Effect of selenium deficiency on the thermoelectric properties of n-type In₄Se_{3-x} compounds, Phys. Rev. B 83 (2011) 115201, doi: 10.1103/PhysRevB.83.115201.
- [32] G. Li, J. Yang, Y. Xiao, L. Fu, Y. Luo, D. Zhang, M. Liu, W. Li, M. Zhang, M.A. White, Effect of TiC nanoinclusions on thermoelectric and mechanical performance of polycrystalline In₄Se_{2.65}, J. Am. Ceram Soc 98 (2015) 3813–3817, doi: 10.1111/jace.13773.
- [33] D.B. Luo, H.G. Si, Y.X. Wang, Electronic structure and thermoelectric properties of In₄Se_{3-x} (X=0, 0.25, 0.5, 0.75): first-principles calculations, J. Alloys Compd. 589 (2014) 125–131, doi: 10.1016/j.jallcom.2013.11.189.
- [34] W. Deng, G. Li, X. Zhang, S.I. Morozov, W.A. Goddard, P. Zhai, The mechanism of deformation and failure of In₄Se₃ based thermoelectric materials, ACS Appl. Energy Mater. (2020), doi: 10.1021/acsaem.9b02103.
- [35] S. Plimpton, Fast parallel algorithms for short-range molecular dynamics, J. Comput. Phys. 117 (1995) 1–19, doi: 10.1006/jcph.1995.1039.
- [36] D.M. Heyes, Pressure tensor of partial-charge and point-dipole lattices with bulk and surface geometries, Phy. Rev. B 49 (1994) 755–764, doi: 10.1103/PhysRevB.49.755.
- [37] A. Stukowski, Structure identification methods for atomistic simulations of crystalline materials, Model. Simul. Mater. Sci. Eng. 20 (2012) 045021, doi: 10.1088/0965-0393/20/4/045021.
- [38] X. Tong, H. Zhang, D.Y. Li, Effect of annealing treatment on mechanical properties of nanocrystalline alpha-iron: an atomistic study, Sci. Rep. 5 (2015) 8459, doi: 10.1038/srep08459.
- [39] L.A. Zepeda-Ruiz, A. Stukowski, T. Oppelstrup, V.V. Bulatov, Probing the limits of metal plasticity with molecular dynamics simulations, Nature 550 (2017) 492– 495, doi: 10.1038/nature23472.
- [40] J. Hogg, H. Sutherland, D. Williams, The crystal structure of tetraindium triselenide, Acta Crystal. Sec. B 29 (1973) 1590–1593.
- [41] D. Bercha, K. Rushchanskii, M. Sznajder, Phonon spectrum of the layered In₄Se₃ crystal, Phys. Status Solidi (b) 212 (1999) 247–261.
- [42] C.M. Sellars, W. McTegart, On the mechanism of hot deformation, Acta Metall. 14 (1966) 1136–1138, doi: 10.1016/0001-6160(66)90207-0.
- [43] Q.-X. Pei, Z.-D. Sha, Y.-Y. Zhang, Y.-W. Zhang, Effects of temperature and strain rate on the mechanical properties of silicene, J. Appl. Phys. 115 (2014) 023519, doi: 10.1063/1.4861736.
- [44] K. Ahn, E. Cho, J.-.S. Rhyee, S. II Kim, S.Mock Lee, K.Hyoung Lee, Effect of cationic substitution on the thermoelectric properties of In_{4-x}M_xSe_{2.95} compounds (M= Na, Ca, Zn, Ga, Sn, Pb; x= 0.1), Appl. Phys. Lett. 99 (2011) 102110, doi: 10.1063/1.3637053.
- [45] K. Ahn, E. Cho, J.-.S. Rhyee, S.I. Kim, S. Hwang, H.-.S. Kim, S.M. Lee, K.H. Lee, Improvement in the thermoelectric performance of the crystals of halogen-substituted In₄Se_{3-x}H_{0.03} (H= F, Cl, Br, I): effect of halogen-substitution on the thermoelectric properties in In₄Se_{3-x}, J. Mater. Chem. 22 (2012) 5730–5736, doi: 10.1039/c2im16369a.
- [46] J.S. Rhyee, K. Ahn, K.H. Lee, H.S. Ji, J.H. Shim, Enhancement of the thermoelectric figure-of-merit in a wide temperature range in In₄Se_{3-x}Cl_{0.03} bulk crystals, Adv. Mater. 23 (2011) 2191–2194, doi: 10.1002/adma.201004739.